Stability of external cavity modes in the Lang-Kobayashi system with large delay

Serhiy Yanchuk[1,*] and Matthias Wolfrum[2,†]

[1] *Humboldt-University of Berlin, Institute of Mathematics, Unter den Linden 6, D-10099 Berlin, Germany*

[2] *Weierstrass Institute for Applied Analysis and Stochastics, Mohrenstrasse 39, D-10117 Berlin, Germany*

(Dated: February 23, 2009)

Abstract

The Lang-Kobayashi model is a system of delay differential equations (DDEs) describing the dynamics of a semiconductor laser under delayed optical feedback. In this paper, we study the stability of so called external cavity modes (ECMs), which are harmonic oscillations corresponding to stationary lasing states. We focus on experimentally relevant situations, when the delay is large compared to the internal time scales of the laser. In this case, both the number of ECMs and the number of critical eigenvalues grows to infinity. Applying a newly developed asymptotic description for the spectrum of linearized DDEs with long delay, we are able to overcome this difficulty and to give a complete description of the stability properties of all ECMs. In particular, we distinguish between different types of weak and strong instabilities and calculate bifurcation diagrams that indicate the regions with different stability properties and the transitions between them.

PACS numbers: 05.45.Jn; 42.65.Sf; 42.55.Px;

[*] yanchuk@math.hu-berlin.de

[†] wolfrum@wias-berlin.de

I. INTRODUCTION

Semiconductor lasers are key elements in many modern optoelectronic systems, generating and processing optical signals at high speed [1, 2]. Depending on the condition of operation, they can show, besides stationary lasing, a huge variety of nonlinear dynamical behavior, including e.g. pulsations of different type and frequency, excitability, or high dimensional chaos. In particular, the presence of optical feedback from a distant mirror has been shown to be the origin of a variety of complicated dynamics. The finite propagation speed of light causes here a delay of the feedback signal, leading to a destabilization of the stationary lasing state. With increasing delay, also the dynamical complexity increases and finally a high-dimensional chaotic behavior can be observed.

The Lang-Kobayashi model [3] for a semiconductor laser with delayed optical feedback has been used extensively to study these dynamical phenomena. In dimensionless form the Lang-Kobayashi model can be written as follows [4–11]

$$\begin{aligned} E'(t) &= (1+i\alpha)n(t)E(t) + \eta e^{-i\varphi}E(t-\tau), \\ n'(t) &= \varepsilon[J - n(t) - (2n(t)+1)|E(t)|^2]. \end{aligned} \tag{1}$$

The equations describe the evolution of the complex electric field $E(t)$ and excess carrier density $n(t)$. The physical meaning of the system parameters is as follows: J is the excess pump current, $\tau > 0$ is the external cavity round trip time measured in the units of the photon lifetime, $\eta > 0$ and φ are the feedback strength and feedback phase, respectively. The presence of the so called *linewidth enhancement factor* α is the main reason for dynamical instability under delayed feedback, which is typical for semiconductor lasers. In experiments, the length of the external cavity can vary from less then 1 mm in monolithically integrated devices up to ~ 1 m in the case of reflection from a distant mirror.

Due to the equivariance with respect to optical phase-shifts $(E, n) \to (Ee^{i\psi}, n)$, periodic solutions of the form $E(t) = ae^{i\omega t}$, $n(t) = N$ appear generically in (1), which are relative equilibria with respect to this symmetry. They are usually called *external cavity modes* (ECMs) and correspond to stationary lasing with a constant relative optical frequency ω. Depending on the choice of the parameters, the ECMs can have different stability properties and can be considered as the starting point for the development of different dynamical regimes [4, 12–14].

The main goal of this paper is to analyze the stability properties of the ECMs in the case of large delay. This is a difficult task, since delay differential equations have an infinite number of eigenvalues and with increasing delay time an increasing number of these eigenvalues become relevant for the issue of stability. Our main tool will be a recently developed theoretical approach to the asymptotic behavior of the spectrum for delay-differential equations with large delay [15–18]. Using this method, we are able to distinguish between eigenvalues with different scaling behavior for $\tau \to \infty$, leading to the notion of strong and weak instability, and to calculate explicit asymptotic approximations for their location. Based on this, we can determine the stability of the ECM solutions, indicate the dimension of the unstable manifolds, and distinguish different types of instability.

The paper is organized as follows. In Sec. II, we introduce some notations and review some basic facts about ECMs. The main results about stability of ECMs will be presented in Sec. III. In particular, we classify all ECMs of the Lang-Kobayashi system accordingly to their stability properties. The resulting classification will reveal: stable ECMs; strongly unstable ECMs of oscillatory or antimode type; weakly unstable ECMs with modulational, Turing-type, or uniform instability.

The fundamental assumption for our analysis is that the delay τ is large. In physical terms, the mathematical limit $\tau \to \infty$ is justified as soon as the delay of optical feedback is larger than the period of the relaxation oscillations, i.e. $\tau \gg T_{RO} \sim 2\pi/\sqrt{2\varepsilon J}$. The obtained results (e.g. bifurcation diagrams) are independent on the actual value of τ and hold as soon as τ is large enough. This fact allows in particular to overcome difficulties arising with the use of standard numerical bifurcation analysis for DDEs, where the condition of the problem is getting worse with large delay.

II. EXTERNAL CAVITY MODES

In this section, we recall some facts about the ECMs of the Lang-Kobayashi system. Substituting $E(t) = ae^{i\omega t}, n(t) = N$ into (1), we obtain for N, ω, and a:

$$N = -\eta \cos(\varphi + \omega\tau), \tag{2}$$

$$\omega - \alpha N = -\eta \sin(\varphi + \omega\tau), \tag{3}$$

$$a^2 = \frac{J - N}{2N + 1}. \tag{4}$$

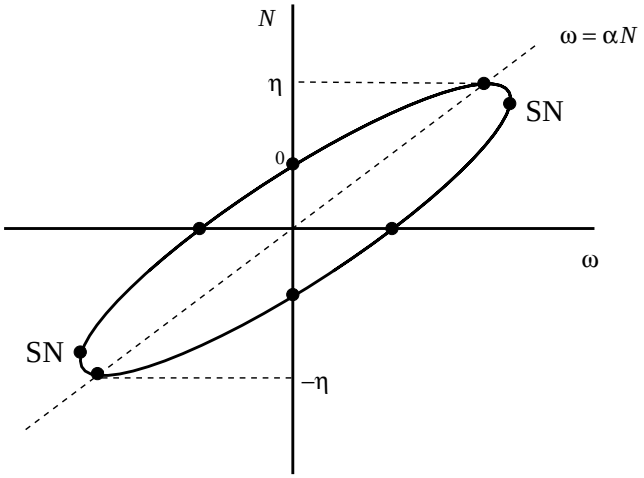

Figure 1: Location (6) of ECMs in the (ω, N)-plane for fixed η and varying φ, τ. SN: Location of saddle-node ECMs; ECMs with maximum and minimum gain at $N = \pm\eta$.

By physical reasons, the Lang-Kobayashi system makes sense only for $0 < \eta \ll 1$. By this reason, the denominator in (4) is positive and we can conclude that

$$N \leq J, \tag{5}$$

in order to obtain a real amplitude a.

From (2) and (3) we obtain

$$N^2 + (\omega - \alpha N)^2 = \eta^2. \tag{6}$$

Hence, for all ECMs the corresponding values ω and N lie on an ellipse (6) of size η, see Fig. 1.

The positions of ECMs on the ellipse are given by solutions ω of the transcendental equation

$$-\eta(\sin(\varphi + \omega\tau) + \alpha\cos(\varphi + \omega\tau)) = \omega, \tag{7}$$

obtained from (2) and (3). The corresponding values of N are given by (2). It is easy to see that the number of ECMs (solutions to (7)) is proportional to $\eta\tau$ and can be estimated as $2\tau\eta\sqrt{1+\alpha^2}$ (see also [19]). For large τ, the ellipse (6) becomes filled densely with ECMs. Varying the feedback phase φ, the position of an individual ECM can be moved along the ellipse and pairs of ECMs are created or annihilated in saddle-node bifurcations. The location of the saddle-node can be found by calculating double roots of (7). Differentiating (7) with respect to ω, we obtain the condition

$$\eta\tau(\cos(\varphi + \omega\tau) - \alpha\sin(\varphi + \omega\tau)) = -1. \tag{8}$$

Using this together with (2) and (3), we obtain the condition for the saddle-node bifurcation in (ω, N)-plane as

$$N(1+\alpha^2) - \alpha\omega = \frac{1}{\tau}. \tag{9}$$

It is a straight line and, if τ or η are large enough, it has two intersections with the ellipse, corresponding to two saddle-nodes. Note that there is a saddle-node bifurcation of ECMs, only if one of these points satisfies additionally (7). This can be understood as follows. Keeping η and τ fixed and varying φ, the ECMs move along the ellipse, being created and annihilated respectively at the two saddle-node points given by these intersections. For increasing τ, consecutive pairs of ECMs are generated at both saddle-node points, see Figure 2. In the limit $\tau \to \infty$, the saddle-node points tend to the rightmost and the leftmost points on the ellipse, compare Fig. 1. At each saddle-node the ECM that emanate to the upper half of the ellipse are of saddle type and remain unstable (see e.g. [19]). They are usually called *antimodes*. The ECMs on the lower part, which under some conditions can be stable, are called *modes*. Note that, according to (4) only the ECMs below the line $N = J$ lead to physically relevant solutions with positive real amplitude a.

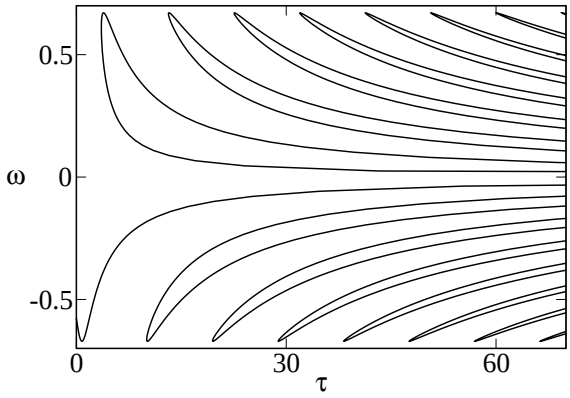

Figure 2: ECM frequencies ω versus delay τ for $\alpha = 2$, $\varphi = 1$, $\eta = 0.3$.

III. STABILITY OF ECMS

Now we will investigate the stability properties of the ECMs. Our primary bifurcation parameters are the feedback parameters η and φ. The third main parameter is the delay time τ. We consider τ to be large and our results will turn out to be independent on the

precise value of τ. As in various papers on the Lang-Kobayashi system we will use, instead of classical bifurcation diagrams, a representation in the (ω, N)-plane. In the previous section we have shown that any ECM is uniquely described by its position in this plane and how this position is related to the feedback parameters η and φ.

ECMs are periodic solutions and their stability is determined by an infinite set of Floquét multipliers. Due to their invariance with respect to the phase shift symmetry they can be considered as relative equilibria. Under the coordinate transformation

$$E \to e^{i\omega t}E,$$

an ECM solution $E = ae^{i\omega t}$, $n = N$ is transformed into a one-parameter family of equilibria $E = ae^{i\rho}$,$n = N$ with the free parameter ρ. In this way, their stability can be analyzed by linearizing the system and computing eigenvalues, i.e. the roots of the characteristic equation. However, one has to regard that a zero eigenvalue will appear, corresponding to perturbations along the family of equilibria. In this way one obtains the characteristic equation (compare [19], [5]):

$$\chi(\lambda) := \det \begin{bmatrix} N(e^{-\lambda\tau}-1)+\lambda & \beta(e^{-\lambda\tau}-1) & -a \\ -\beta(e^{-\lambda\tau}-1) & N(e^{-\lambda\tau}-1)+\lambda & -\alpha a \\ 2a\varepsilon(2N+1) & 0 & \varepsilon(1+2a^2)+\lambda \end{bmatrix} = 0. \qquad (10)$$

We have used the abbreviation $\beta = \omega - \alpha N$, and the expression (4) for the amplitude a of the corresponding ECM. This characteristic equation should be understood as follows. Fixing the laser parameters $\alpha, \varepsilon, \tau$ we obtain the eigenvalues for any ECM by inserting the corresponding parameters ω, N, and a. In this way, the values of the bifurcation parameters are entering implicitly equations (2) – (4).

Figure 3 shows some typical spectra of eigenvalues for ECMs at different positions on the ellipse, i.e. for fixed η, fixed large delay, and different values of φ. One can observe that most of the eigenvalues accumulate along two curves of varying shape. It turns out that this behavior is typical for delay-differential equations with large delay and can be understood by some recently developed asymptotic approach [15–18]. The curves in Figure 3 where obtained by the asymptotic formulas which will be presented in the next section.

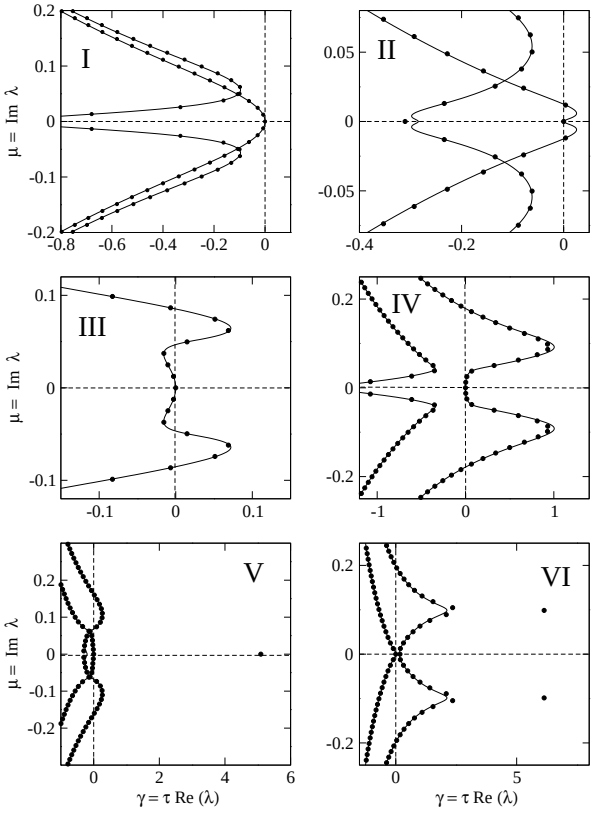

Figure 3: Typical spectra of ECMs. Points: numerically computed eigenvalues; Lines: analytical curves of pseudo-continuous spectrum. Parameter values: $\tau = 500$, $\eta = 0.1$, $\varepsilon = 0.01$, $J = 0.01$. Depending on the position of the ECM on the ellipse (6), qualitatively different types of spectra appear: (I): asymptotically stable ECM; (II) and (IV): weak modulational type instability; (III): Turing-type instability with rotational invariance; (V): strong antimode instability; (VI): strong oscillatory instability.

IV. ASYMPTOTIC PROPERTIES OF SPECTRUM

In this section we briefly recall some ideas for the asymptotic approximation of the eigenvalues of stationary states of a delay-differential equation in the limit of large delay [15–18]. Let be

$$x'(t) = Ax(t) + Bx(t-\tau), \quad x \in \mathbb{R}^n \tag{11}$$

a linear system of DDEs, where the matrices A and B should be considered as the Jacobians with respect to the instantaneous and the delayed variables for a given fixed point of a

nonlinear DDE. The characteristic equation reads as

$$\det(\lambda I + A + Be^{-\lambda\tau}) = 0, \tag{12}$$

where I is the identity matrix. As shown in [15–18], the spectrum can be decomposed into two parts with different scaling properties with respect to τ: *pseudo-continuous* spectrum, which scales as $\mathrm{Re}\,(\lambda) \sim 1/\tau$, and *strongly unstable* spectrum, which scales as $\mathrm{Re}\,(\lambda) \sim 1$ for large τ. The strongly unstable spectrum asymptotically coincides with the unstable part of the spectrum of the instantaneous part of the equation, i.e. the equation without feedback $x' = Ax$ and satisfies

$$\det(A - \lambda I) = 0, \quad \mathrm{Re}\,(\lambda) > 0. \tag{13}$$

The pseudo-continuous spectrum is obtained by introducing the scaling

$$\lambda = \frac{\gamma}{\tau} + i\mu \tag{14}$$

with the real parameters γ and μ. Inserting this into Eq. (12), we obtain in leading order the equation

$$\det\left(-i\mu I + A + Be^{-\gamma}e^{i\Phi}\right) = 0, \tag{15}$$

where we have introduced $\Phi = -\frac{\mu}{\tau}$. Note that for large τ the term $e^{i\Phi}$ is rapidly oscillating in μ. Based on this observation, we consider Φ as an artificial phase parameter and determine the solution to (15) as a curve in the (γ, μ)-plane that is parametrized by Φ. In fact, it is even possible to eliminate Φ and obtain this curve by expressing γ as a function of μ. To this end, we have to calculate the roots of a polynomial with the degree given by the number of delayed variables and obtain a corresponding number of solution branches $\gamma_j(\mu)$. Below, we show in detail how in this way one can obtain the curves in Figure 3 for the Lang-Kobayashi system. Note that the calculation of these branches is extremely simplified with respect to the original problem and moreover is independent on the singular parameter τ. To recover the location of the eigenvalues one has to regard the scaling ansatz (14). Additionally, one needs some information about the actual positions of the eigenvalues along this curve. For our purpose here it is sufficient to notice that, again to leading order, the distance of eigenvalues along the curves behaves like $2\pi k/\tau$ (for more details, see [15–18]). This shows that, using the scaling (14), in the limit of large τ the eigenvalues accumulate along the curves given by (15), while their distance tends to zero. By this reason, we call the set of

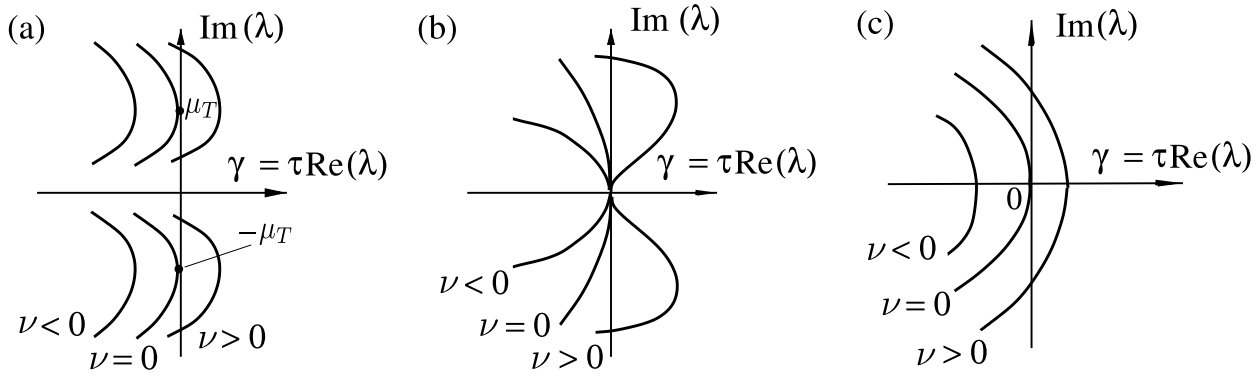

Figure 4: Different destabilization scenarios in delay systems with long delay, caused by bifurcations of the pseudo-continuous spectrum. (a) Turing instability, (b) modulational instability, (c) uniform instability. Stability for bifurcation parameter $\nu < 0$, instability for $\nu > 0$.

eigenvalues behaving in this way *pseudo-continuous spectrum (PCS).* It turns out that, in general, all eigenvalues are either part of the strongly unstable or of the pseudo-continuous spectrum. Moreover, one can show that the destabilization of a stationary state happens always through a branch of PCS moving through the imaginary axis. Note that in such cases immediately a large number of eigenvalues crosses the imaginary axis, and a description of the destabilization scenario in terms of classical bifurcation theory is valid only in a region of asymptotically small size. Instead, a description of the occurring instabilities in analogy to spatially extended systems is much more appropriate and has already been applied by several authors, e.g. [17, 20–23] .

As for instabilities of spatially extended systems, one has to distinguish different types of instabilities, depending on the shape of the branch that moves through the imaginary axis: modulational instability, Turing instability, and uniform instability, see Fig. 4.

We call these instabilities weak, since after destabilization the real parts of the involved eigenvalues are of order $1/\tau$, leading to correspondingly slow divergence rates. At the same time, there is a large number of weakly unstable eigenvalues located on the unstable part of the pseudo-continuous spectrum. As a result, a weakly unstable stationary state will possess a high-dimensional unstable manifold, whose dimension is proportional to the large delay. In contrast to that, the presence of strongly unstable spectrum implies a strong divergence in a low-dimensional unstable manifold.

V. INSTABILITIES IN THE LANG-KOBAYASHI SYSTEM

In this chapter, we will give a complete description of the stability properties of the ECM solutions in the case of large delay, using the asymptotic approach explained in the previous chapter. As a final result we will present a partition of the (ω, N)-plane in different regions where the spectra behave qualitatively like one of the examples in Figure 3. The transitions between these regions will be described by bifurcation curves where a specific singular behavior of the spectrum can be observed.

In order to calculate the strongly unstable part of the spectrum. According to to (13), we have to use only the instantaneous terms

$$\det \begin{bmatrix} N-\lambda & \beta & a \\ -\beta & N-\lambda & \alpha a \\ -2a\varepsilon(2N+1) & 0 & -\varepsilon(1+2a^2)-\lambda \end{bmatrix} = 0 \tag{16}$$

from (10) and solve for solutions with positive real part.

The pseudo-continuous spectrum is given by the two solution branches

$$\gamma_j(\mu) = -\ln|Y_j(\mu)|, \quad j = 1, 2, \tag{17}$$

where the complex valued functions $Y_j(\mu)$ satisfy the equation

$$\det \begin{bmatrix} N(Y-1)+i\mu & \beta(Y-1) & -a \\ -\beta(Y-1) & N(Y-1)+i\mu & -\alpha a \\ 2\varepsilon(1+2N)a & 0 & \varepsilon(1+2a^2)+i\mu \end{bmatrix} = 0, \tag{18}$$

which has been obtained by inserting $Y(\mu) := e^{-\gamma}e^{i\Phi}$ and the corresponding Jacobians for A and B into (15).

A. Stable ECMs

At first, we show that a small part of ECMs with low N is asymptotically stable. We prove this by showing the stability of the so called maximum gain ECM at the bottom of the ellipse, i.e $N = -\eta$ (compare Fig. 1) . Stability for a set of neighboring ECMs follows then by continuity arguments and asymptotic closeness of ECMs on the ellipse for large τ. The

maximum gain ECM is given by $\omega = \alpha N$, or $\beta = 0$. After substituting this into Eq. (18), the characteristic equation factorizes and we obtain for the PCS

$$[N(Y-1)+i\mu]\cdot\left[2\varepsilon(J-N)+(\varepsilon(1+2a^2)+i\mu)(N(Y-1)+i\mu)\right]=0.$$

Solving for Y and taking into account that $N=-\eta$ for this ECM, we obtain from the first factor the solution branch

$$Y_1(\mu)=1+i\frac{\mu}{\eta} \tag{19}$$

and from the second

$$Y_2(\mu)=1+i\frac{\mu}{\eta}+\frac{2\varepsilon(J+\eta)[\varepsilon(1+2a^2)-i\mu]}{\eta(\mu^2+\varepsilon^2(1+2a^2)^2)}. \tag{20}$$

Taking into account that η, ε, and $J-\eta$ are positive quantities, one can find easily that $|Y_2(\mu)|>1$ and $|Y_1(\mu)|\geq 1$ for all μ. According to (17), the corresponding PCS curves satisfy $\gamma_{1,2}(\mu)\leq 0$ that implies stability with respect to the PCS. In order to look for strong instabilities, we have to insert $\beta=0$ and $N=-\eta$ into (16) and check whether there are solutions with positive real part. Again we obtain the characteristic equation in a factorized form

$$(\lambda+\eta)(\lambda^2+\lambda(\varepsilon(1+2a^2)+\eta)+\varepsilon\eta(1+2a^2)+2\varepsilon a^2(1-2\eta))=0.$$

By a straight forward application of the Routh-Hurwitz criterion, we conclude that there are no positive roots and hence no strong instabilities. Since the property of asymptotic stability is robust under small perturbations, the same holds for all ECMs which are close enough to the maximum gain ECM. In Fig. 3(I) we show a plot of corresponding PCS curves together with the numerically computed eigenvalues for some fixed value of τ. In Fig. 11 the region of stability is shown in white. We will now determine the boundary of this region by calculating the conditions for different types of instabilities.

B. Weak modulational instability

It turns out that one of the stability boundaries is given by a *weak modulational instability*, compare Fig. 3(IV) and Fig. 4 (b). It occurs when the curvature of the PCS branch that is pinned to the origin by symmetry becomes positive there, i.e. $\gamma_j''(0)>0$. The condition for the corresponding stability boundary is given by

$$\gamma_j''(0)=0.$$

Using Eq. (18), we obtain for the function $Y_1(\mu)$ near the origin the expansion:

$$Y_1(\mu) = 1 + \kappa_1\mu + \kappa_2\mu^2 + O(\mu^3), \quad \text{where}$$

$$\kappa_1 = \frac{i}{\alpha\beta - N} \quad \text{and} \quad \kappa_2 = \frac{\beta^2(1+\alpha^2)(1+2J)}{2(\alpha\beta - N)^3(1+2N)(J-N)}.$$

Taking into account (17), we have for the function $\gamma_1(\mu)$

$$\gamma_1(\mu) = c_2\mu^2 + O(\mu^3),$$

where

$$c_2 = \kappa_2 - \frac{1}{2}\left(\frac{1}{\alpha\beta - N}\right)^2. \tag{21}$$

The condition $\gamma_1''(0) = 0$ is equivalent to $c_2 = 0$. This yields

$$(1+\alpha^2)\beta^2\frac{1+2J}{1+2N} = (J-N)(\alpha\beta - N) \tag{22}$$

as the condition for the onset of weak modulational instability. In Figure 5 the region of ECMs with weak modulational instability are shown. There is destabilization of stable ECMs by the onset of modulational instability and also, as we will show later, transition from Turing-unstable to modulationally unstable ECMs. Additionally, there is a transition from modulational instability to uniform instability by a branch-switching as indicated in Fig. 6. In this scenario the stable second branch of PCS approaches the origin as well and both branches merge there, before the unstable branch detaches itself from the origin and exhibits a uniform instability. As the condition for this transition we obtain the expression

$$N - \alpha\beta = 0. \tag{23}$$

by inserting $\tau = \infty$ into the saddle-node condition (9). Note that inserting this into (21) leads to $c_2 = \infty$, i.e. the curvature of the branches in Fig. 6 (middle) as a function $\gamma(\mu)$ is infinite. From Eq. (22) we obtain that the curve for the onset of modulational instability is always in the region below the asymptotic saddle node line (23) where $N - \alpha\beta < 0$. This follows immediately from the fact that both, the left-hand side of Eq. (22), and $J - N$ are positive. From this we can conclude that the saddle-node bifurcation SN does not produce a pair of stable and unstable ECM, but rather two unstable ECMs. Moreover, at a sufficiently long delay, ECMs already have high-dimensional weakly unstable manifold at the SN point. This is in contrast to the short delay regime, where at SN point a pair of stable and unstable ECMs appears.

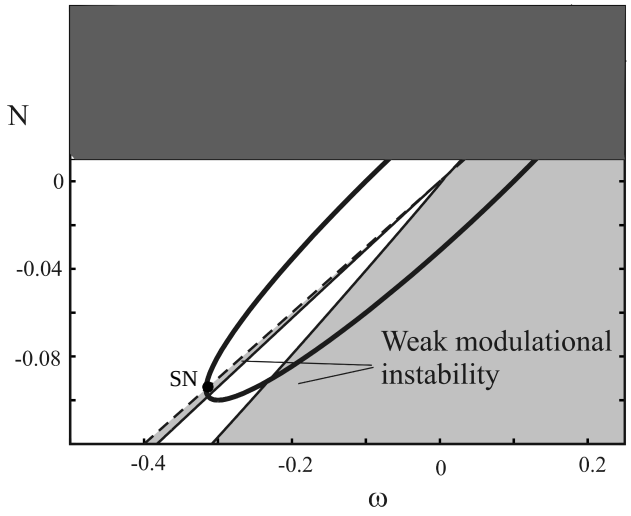

Figure 5: Region of weak modulational instability (gray area) in the $(\omega.N)$-plane, enclosed by (22) and branch-switching (dashed), given by (23). Bold curve: ellipse of ECMs for $\eta = 0.1$. There are no ECMs in the region $N > J = 0.01$; $\alpha = 3$.

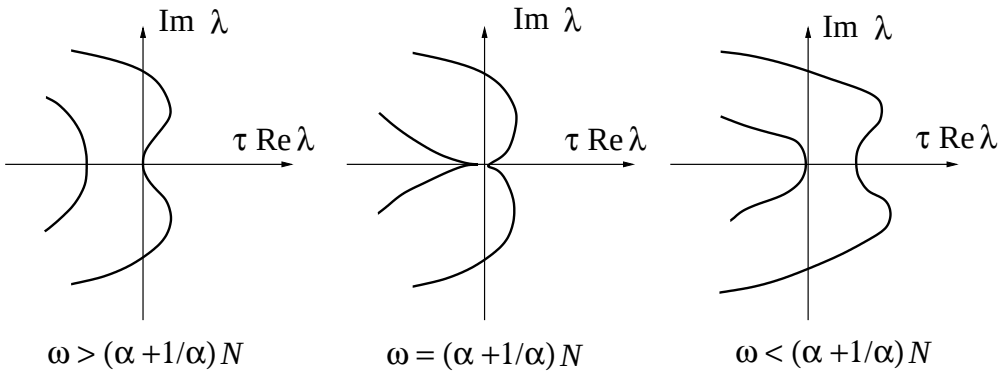

Figure 6: Transition form modulational to uniform instability by branch-switching.

C. Weak Turing instability

A weak Turing instability occurs when a branch of pseudo-continuous spectrum touches the imaginary axis and the interval of frequencies $0 < \mu_- < \mu < \mu_+ < \infty$ is destabilized, cf. Fig. 3(III).

For a given branch $\gamma(\mu)$ of the pseudo-continuous spectrum, the condition for the onset of Turing instability is

$$\gamma'(\mu_T) = 0, \quad \gamma(\mu_T) = 0, \quad \mu_T \neq 0. \tag{24}$$

Since analytic expressions are becoming non tractable, we solve the system (24) together

with (18) numerically. By a continuation procedure we can find solution curves $\omega(N)$ for a fixed choice of parameters α and a. The result of such a continuation is given by the solid line (T) in Fig. 7. Together with the dashed line (M), where the Turing instability is transformed into a modulational instability, it constitutes the boundary of the region of Turing-unstable ECMs. The dynamics in the vicinity of such ECMs is determined by a large number of weakly unstable eigenmodes which are located close to the relaxation frequency of the solitary laser. This situation, where the oscillation mode of the solitary laser is split into a number of resonances by the delayed feedback has already been described in [13].

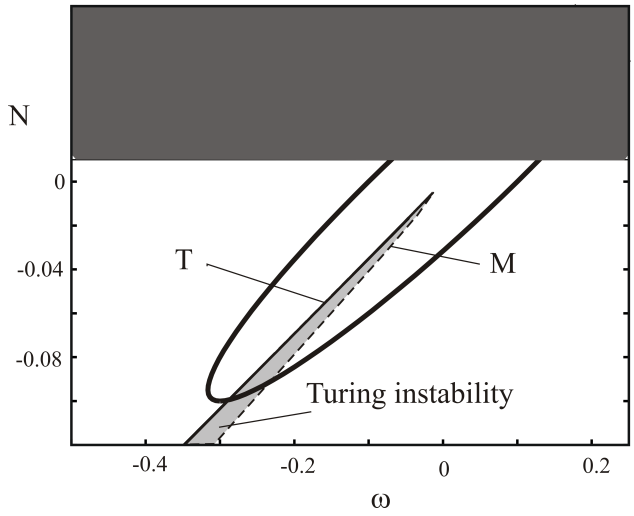

Figure 7: Region of weak Turing-instability in the plane (ω, N) (gray), enclosed by the curve (24) (T), and a transition to modulational instability (M), cf. Fig.5.

D. Weak uniform instability

The *weak uniform instability* occurs when a branch of the pseudo-continuous spectrum is positive $\gamma_j(\mu) > 0$ for some interval $-\mu_0 < \mu < \mu_0$, where $\mu_0 > 0$, cf. 4(c). Recalling that as a result of the phase-shift invariance one branch of the pseudo-continuous spectrum passes always through the origin, the condition for the onset of weak uniform instability is

$$\gamma_{1,2}(0) = 0$$

i.e. both branches meet the origin. Using Eq. (17), this requires either $Y_j = 1$ or $Y_j = -1$. The first condition is satisfied at the saddle-node point (23) where the branch-switching

transition from modulational to uniform instability takes place. The second condition $Y_j = -1$ describes a transition to uniform instability without a branch-switching and leads to the condition

$$N^2 + \beta^2 + \frac{1+2N}{1+2J}(J-N)(\alpha\beta - N) = 0. \tag{25}$$

Combining Eqs. (23) and (25), we obtain a region of weak uniform instability, which is shown in Fig. 8.

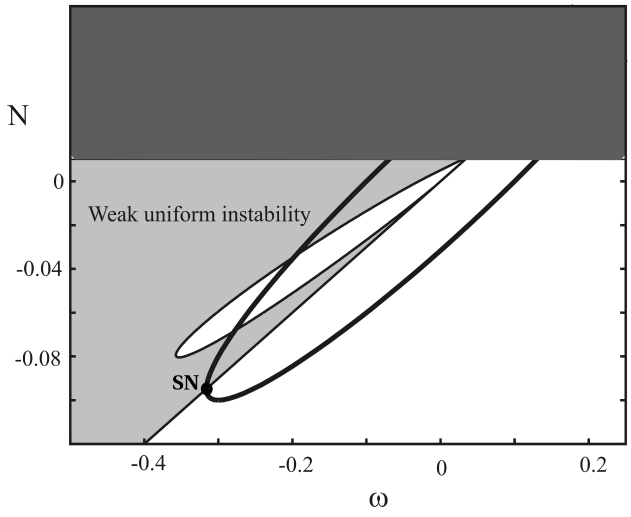

Figure 8: Region of weak uniform instability in the plane (ω, N) (gray area); the boundary is given by (25) and (23), cf. Fig. 5.

E. Strong antimode instability

As we already mentioned above, any destabilization in systems with large delay is mediated by the PCS. Consequently, the onset of a strong instability is always a transition from weak to strong instability. *Strong antimode instability* we call the occurrence of an eigenvalue λ which is real with $\lambda > 0$ and behaves asymptotically as $\lambda = O(1)$ for large τ. Figure 3(V) shows the spectrum of an ECM with such an instability: One leading real eigenvalue can be observed. In order to obtain the corresponding condition for the onset of this type of strong instability, we have to look for solutions $\lambda = 0$ of (16). This leads to the condition

$$N^2 + \beta^2 + 2\frac{1+2N}{1+2J}(J-N)(\alpha\beta - N) = 0. \tag{26}$$

Arguing similarly as above, we can find that this stability boundary is always located in the half-plane above the asymptotic saddle-node line (23), i.e in the region where $N - \alpha\beta > 0$.

In Fig. 9 we have plotted condition (26) after substituting $\alpha = 3$ and $J = 0.01$ and solving with respect to $\omega(N)$. The obtained curves delineate a region, where strong antimode instability occurs. In Fig. 9, this region is shown in gray. Before the onset of this instability, the ECMs are already weakly uniform unstable. The weak uniform instability originates from the branch-switching (23). Recalling from (6) that $\eta^2 = N^2 + \beta^2$, one can observe that, according to Eq. (26), the distance from the branch-switching to the strong antimode instability is of order η^2, i.e. it decreases quadratically for small values of η. By this reason we interpret this instability as the principal origin of the instability of the antimodes in the upper half of the ellipse and call it *strong antimode instability*.

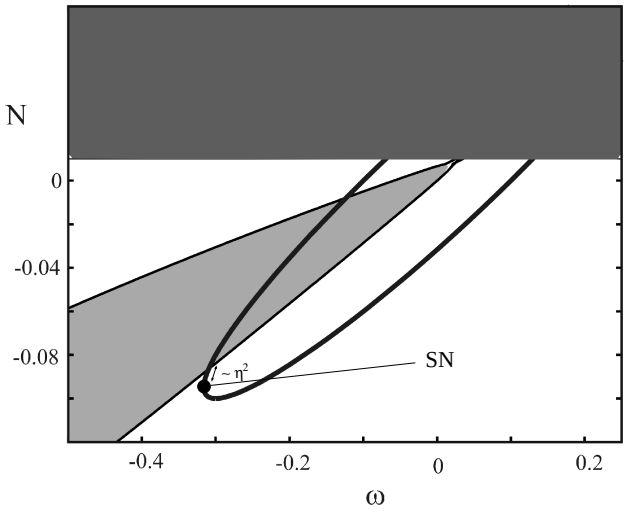

Figure 9: Region of strong antimode instability in the (ω, N)-plane (gray). The distance to the onset of weak uniform instability at the asymptotic saddle-node (SN) is of order η^2.

The dynamics in the neighborhood of the strongly unstable antimodes is determined by the leading unstable characteristic root. Therefore, the orbit, which starts in the vicinity of such ECM will be repelled along a one-dimensional strong unstable manifold on a time scale which is faster than the delay time τ. In addition, it is interesting to note that the condition (26) for this instability is independent on the parameter ε.

F. Strong oscillatory instability

Strong oscillatory instability occurs when a pair of characteristic roots $\lambda_{1,2} = \gamma \pm i\Omega$ with $\gamma > 0$ and $\Omega \neq 0$ appears, and the real part scales as $\gamma = O(1)$ for $\tau \to \infty$. Figure Fig. 3(VI) shows an example of such a spectrum. According to (13), the strongly unstable eigenvalues are approximately given by eigenvalues $\lambda_{1,2} = \gamma \pm i\Omega$ with positive γ of the instantaneous characteristic equation (16). The condition for the onset of this instability can be found by inserting $\lambda = i\Omega$ into (16). Separating real and imaginary parts, the frequency Ω can be eliminated as

$$\Omega = N^2 + \beta^2 + 2\varepsilon(a^2 - N), \tag{27}$$

leading to the condition

$$N(N^2 + \beta^2) + \varepsilon \frac{J - 2N(N+1)}{1 + 2N} \left[2N - \varepsilon \frac{1 + 2J}{1 + 2N} \right] + \varepsilon(J - N)(\alpha\beta - N) = 0. \tag{28}$$

Figure 10 illustrates the region of strong oscillatory instability (gray area). The boundary of this region, is a solution to (28). One can notice, that the strong oscillatory instability appears mainly for ECMs with positive inversion N. Indeed, the condition (28) can be further simplified by taking into account the scaling of other parameters. For instance, if $\varepsilon \ll \eta$ and $\varepsilon \ll \omega$, we obtain the approximation $N \approx \varepsilon J\alpha/\omega$ as a criterion for the occurrence of the strong oscillatory instability.

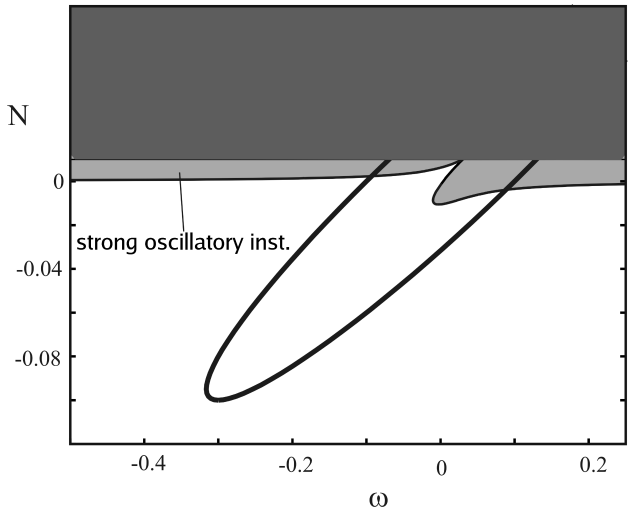

Figure 10: Region of strong oscillatory instability in the (ω, N)-plane, determined by Eq. (28) (gray area).

The dynamics in the neighborhood of the strongly oscillatory unstable ECMs are determined by the leading pair of unstable characteristic roots $\lambda_{1,2} = \gamma \pm i\Omega$, $\gamma > 0$. Therefore, an orbit, which starts in the vicinity of such ECM will be repelled along the two-dimensional unstable manifold exhibiting oscillatory behavior with the frequency Ω. The time of escaping is much less than the round-trip time τ like in the case of antimode instability.

G. Combined stability map of ECMs and primary destabilization mechanisms

Collecting together the results from the preceding sections, we show in Fig. 11 the global picture for the regions with different stability properties (cf. Figs. 5–10).

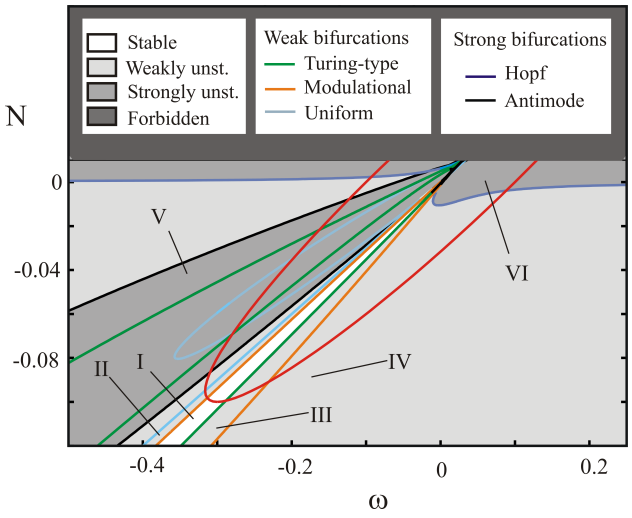

Figure 11: Combined stability map for ECMs. The numbers I to VI denote the type of spectrum for the corresponding region. Corresponding spectra are given in Fig. 3.

Based on this rather complicated picture, we can summarize the following main observations and results:

- There is a region of stable ECMs around the maximum gain mode (I).
- On the lower part of the ellipse (modes), the stable region is followed by a large weakly unstable region. The stability boundary is given by a Turing instability (III), which is followed by a transition to modulational instability (IV).
- The ECMs on the upper part (antimodes) are mainly strongly unstable. In a rather small region close to the maximum gain mode, first a weak modulational instability

(II) appears which, after a transition to uniform instability transforms into a strong antimode-instability (V).

- In the region close to $N = 0$, a strong oscillatory instability (VI) can be observed, both for modes and antimodes.

Note that this global picture can provide a more detailed understanding of the well known low-frequency-fluctuations [12]. In this regime, the solutions move close to the weakly unstable ECMs along the lower part of the ellipse. The high dimensional chaotic behavior along this itinerary is governed by the high dimensional weakly unstable manifolds of the weakly unstable ECMs. Finally, they come close to the maximum gain mode, where the influence of the nearby strong instability leads to the well-known power dropout.

VI. CONCLUSIONS

Using a new asymptotic approach for delay equations with large delay, we have studied in detail the stability properties of the ECM solutions of the Lang-Kobayashi system. Equations (16) – (18) provide simple asymptotic expressions for the location of infinitely many eigenvalues and describe two different types of their scaling behavior for large delay τ. In contrast to earlier works we use no further scaling assumptions except that the delay time τ is large. Based on these asymptotic expressions for the location of the spectrum, we are not only able to describe the stability properties of a single ECM solution, but also to find conditions for the transition between stability an different types of instability. Since the destabilization in delay equations with large delay involve a large number of eigenvalues, we can classify different types of instabilities in analogy to spatially extended systems.

Acknowledgments

This work was supported by DFG (Sonderforschungsbereich 555 "Komplexe nichtlineare Prozesse" and Research center Matheon "Mathematics for key technologies").

---

[1] J. Piprek, ed., *Optoelectronic devices* (Springer-Verlag, New York., 2005).

[2] B. Krauskopf and D. Lenstra, eds., *Fundamental Issues of Nonlinear Laser Dynamics*, no. 548 in AIP Conf. Proc. (AIP, New York, 2000).

[3] R. Lang and K. Kobayashi, IEEE J. Quantum Electron. **16**, 347 (1980).

[4] A. M. Levine, G. H. M. van Tartwijk, D. Lenstra, and T. Erneux, Phys. Rev. A **52**, R3436 (1995).

[5] M. Wolfrum and D. Turaev, Opt. Commun. **212**, 127 (2002).

[6] S. Yanchuk, K. R. Schneider, and L. Recke, Phys. Rev. E **69**, 056221 (2004).

[7] P. M. Alsing, V. Kovanis, A. Gavrielides, and T. Erneux, Phys. Rev. A **53**, 4429 (1996).

[8] M. Peil, T. Heil, I. Fischer, and W. Elsäßer, Phys. Rev. Lett. **88**, 174101 (2002).

[9] T. Heil, I. Fischer, and W. Elsäßer, Phys. Rev. E **58**, R2672 (1998).

[10] J. Mulet and C. R. Mirasso, Phys. Rev. E **59**, 5400 (1999).

[11] V. Z. Tronciu, H.-J. Wünsche, M. Wolfrum, and M. Radziunas, Phys. Rev. E **73**, 046205 (2006).

[12] R. L. Davidchack, Y.-C. Lai, A. Gavrielides, and V. Kovanis, Phys. Rev. E **63**, 056206 (2001).

[13] A. Ritter and H. Haug, J. Opt. Soc. Am. B/ **10**, 130 (1993).

[14] A. Ritter and H. Haug, J. Opt. Soc. Am. B **10**, 145 (1993).

[15] S. Yanchuk and M. Wolfrum, in *ENOC-2005, Eindhoven, Netherlands, 7-12 August 2005* (2005).

[16] S. Yanchuk, Math. Methods Appl. S **28**, 363 (2005).

[17] M. Wolfrum and S. Yanchuk, Phys. Rev. Lett. **96**, 220201 (2006).

[18] S. Yanchuk, M. Wolfrum, P. Hövel, and E. Schöll, Phys. Rev. E **74**, 026201 (2006).

[19] J. Mørk, B. Tromborg, and J. Mark, IEEE J. Quantum Electron. **28**, 93 (1992).

[20] M. Nizette, Phys. Rev. E **70**, 056204 (2004).

[21] S. A. Kashchenko, Computational Mathematics and Mathematical Physics **38**, 443 (1998).

[22] S. A. Kashchenko, Siberian Mathematical Journal **40**, 483 (1999).

[23] A. Politi, F. Ginelli, S. Yanchuk, and Y. Maistrenko, Physica D **224**, 90 (2006).